

Giant Vesicles under Flows: Extrusion and Retraction of Tubes

O. Rossier,* D. Cuvelier, N. Borghi, P. H. Puech, I. Derényi, A. Buguin, P. Nassoy, and F. Brochard-Wyart

Groupe Surfaces douces, Laboratoire PhysicoChimie Curie UMR 168 CNRS / Institut Curie, 26, rue d'Ulm, 75005 Paris, France

Received July 13, 2002. In Final Form: November 7, 2002

The formation of membrane tubes (or tethers), which is a crucial event in many biological processes, is intrinsically a dynamic process. In this paper, we discuss both theoretically and experimentally the dynamical laws that govern extrusion and retraction of tubes extracted from lipid vesicles at high speed and under strong flows. A detailed description of the tether shape provides the first evidence that the tension along the tube increases from the vesicle body to the tip of the tube, while the tube radius decreases. As the pulling force is suppressed suddenly, the tube can relax only from the free end, and the velocity of retraction is a direct measurement of the frozen tension along the tube. We also report experiments on tethers pulled out either by mechanical point-forces or by hydrodynamic (electroosmosis-induced) flow, and we show that the observed dynamical laws for retraction are in good quantitative agreement with our theoretical predictions.

I. Introduction

A point-force acting on the fluid membrane of a living cell or an artificial vesicle is known to give rise to the extraction of thin bilayer tubes from the membrane.¹ A large variety of tether-pulling experiments have been reported during the past decade using mechanical micropipet manipulation,^{2–4} optical tweezers,⁵ electrical microelectrode manipulation,^{6,7} or growth of rigid biopolymers such as microtubules inside vesicles.^{8,9} The possibility of obtaining calibrated tubes of diameters in the submicronic range is found to be very promising in the fabrication of micro/nanofluidic devices or nanocircuits and networks used as integrated cellular biosensors.^{6,7,10} The statics of these tubular structures is now well understood from a theoretical point of view,² and all experiments taken together provided accurate and useful values of the mechanical properties of bilayer membranes^{11,12} as well as new insight into cell membrane elasticity⁵ and into membrane–cytoskeleton coupling.¹³ More recently, the phase diagram of vesicle deformation induced by axial load and the initial formation of fluid nanotubes have been investigated theoretically by various groups.^{14–16} Tubular networks have also been observed in living cells.

Some biological membranes (such as the endoplasmic reticulum, the Golgi apparatus, or the inner mitochondrial membrane) often exhibit hairy structures involved in the intracellular transport.^{17,18} These narrow ramifications are pulled by kinesin motor proteins, and their structure is highly dynamic.¹⁹ However, the dynamical laws for growth and retraction of these intrinsically dynamic tubes have often been overlooked.

In the present paper, our purpose is to specifically study the dynamical features of fluid bilayer filaments extracted from giant vesicles. To our knowledge, the unique work dealing with the dynamics of tether extrusion is due to Evans et al.² First, we shall present a theoretical background of tube formation and a reminder of the Evans results. Then, we will provide detailed theoretical predictions about the extrusion, shape, and retraction of tubes when they are pulled out either by point-forces (section III) or by an overall hydrodynamic flow (section IV). Finally, in section V, we describe and analyze experimental observations of retracting tubes. Two different situations are considered. Extrusion of tethers was achieved either by mechanical micropipet pulling or by an electroosmotic flow. We demonstrate that the temporal shrinkage of tube length (when the external force is suppressed) strongly depends on the way tubes were formed, and we show that observed retraction dynamics are in good agreement with our theoretical predictions.

II. Theoretical Background

1. Static Properties of Fluid Tubes. The formation of tubes when a vesicle is stretched can be understood as a first-order transition at a certain threshold force f_c .^{15,16} The following, simple argument shows this. Let us assume

* To whom correspondence and requests for materials should be addressed. E-mail: olivier.rossier@curie.fr.

- (1) Waugh, R. *Biophys. J.* **1982**, *38*, 29–37.
- (2) Evans, E.; Yeung, A. *Chem. Phys. Lipids* **1994**, *73*, 39–56.
- (3) Yeung, A. Ph.D. Thesis, Physics Department, University of British Columbia, Canada.
- (4) Waugh, R. E.; Mantalaris, A.; Bauserman, R. G.; Hwang, W. C.; Wu, J. H. D. *Blood* **2001**, *97*, 1869–1875.
- (5) Dai, J.; Sheetz, M. P. *Biophys. J.* **1999**, *77*, 3363–3370.
- (6) Karlsson, M.; Sott, K.; Cans, A.-S.; Karlsson, A.; Karlsson, R.; Orwar, O. *Langmuir* **2001**, *17*, 6754–6758.
- (7) Karlsson, R.; Karlsson, M.; Karlsson, A.; Cans, A.-S.; Bergenholtz, J.; Akerman, B.; Ewing, A. G.; Voinova, M.; Orwar, O. *Langmuir* **2002**, *18*, 4186–4190.
- (8) Fygenson, D. K.; Elbaum, M.; Shraiman, B.; Libchaber, A. *Phys. Rev. E* **1997**, *55*, 850–859.
- (9) Fygenson, D. K.; Marko, J. F.; Libchaber, A. *Phys. Rev. Lett.* **1997**, *79*, 4497–4500.
- (10) Evans, E.; Bowman, H.; Leung, A.; Needham, D.; Tirrell, D. *Science* **1996**, *273*, 933–935.
- (11) Song, J.; Waugh, R. *Biophys. J.* **1993**, *64*, 1967–1970.
- (12) Raphael, R.; Waugh, R. *Biophys. J.* **1996**, *71*, 1374–1388.
- (13) Hochmuth, R. M.; Marcus, W. D. *Biophys. J.* **2002**, *82*, 2964–2969.

(14) Heinrich, V.; Bozic, B.; Svetina, S.; Zeks, B. *Biophys. J.* **1999**, *76*, 2056–2071.

(15) Derényi, I.; Julicher, F.; Prost, J. *Phys. Rev. Lett.* **2002**, *88*, 238101.

(16) Powers, T. R.; Huber, G.; Goldstein, R. E. *Phys. Rev. E* **2002**, *65*, 041901.

(17) Lee, C.; Chen, L. B. *Cell* **1988**, *54*, 37–46.

(18) Mollenhauer, H. H.; Morre, D. J. *Histochem. Cell. Biol.* **1998**, *109*, 533–543.

(19) Roux, A.; Cappello, G.; Cartaud, J.; Prost, J.; Goud, B.; Bassereau, P. *PNAS* **2002**, *99*, 5394–5399.

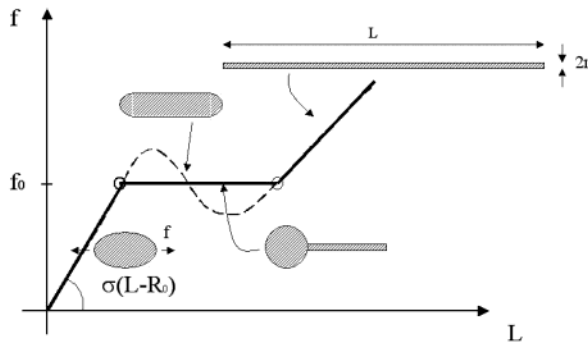


Figure 1. Schematic plot of force f versus elongation L of a vesicle of initial radius R_0 and a constant tension σ . At small forces, the vesicle has an ellipsoidal shape and the force is proportional to $L - R_0$. Under strong forces, the shape becomes a “cigar” of length L and radius r . The force f decreases with elongation L : this region is unstable and corresponds to the Rayleigh instability of a cylindrical vesicle. At intermediate force $f = f_0 = f_c$, we have a coexistence between a quasispherical vesicle and a tether.

that the tension σ of the vesicle is constant and that the volume Ω is fixed. When it is stretched by two opposite distributed forces in a “Gedanken” experiment (Figure 1), we assume that the vesicle is elongated. The shape is ellipsoidal at small forces. If L is the length along the long axis and R_0 the initial radius, the force is proportional to $L - R_0$ ($f \approx \sigma(L - R_0)$). Under strong forces, the shape becomes a “cigar” of length L and radius r . Neglecting end cap effects ($r/L \ll 1$), the energy of the cylindrical vesicle is the sum of the curvature and surface energies

$$\frac{F}{2\pi} = \frac{1}{2} \frac{K}{r^2} L + \sigma L \quad (1)$$

where K is the bending rigidity ($K \approx 4 \times 10^{-20}$ J).

With the conservation of the volume

$$\pi r^2 L = \Omega \quad (2)$$

we can eliminate r and calculate the force $f = \partial F / \partial L$ from eq 1.

$$\frac{f}{2\pi} = \frac{3}{4} K \frac{L^{1/2} \pi^{1/2}}{\Omega^{1/2}} + \frac{1}{2} \sigma \frac{\Omega^{1/2}}{L^{1/2} \pi^{1/2}} = \frac{3}{4} \frac{K}{r} + \frac{1}{2} \sigma r \quad (3)$$

We show in Figure 1 a schematic plot of the force versus the elongation L : in the case of liquid droplets, the decrease of f versus L is related to the Rayleigh instability of a liquid cylinder. Here, by contrast, for $f = f_c$, we have coexistence between a quasispherical vesicle and a thin tube. The pressure in the two compartments is equal. The pressure inside the sphere is $P = 2\sigma/R_0 \approx 0$. Inside the tube, the pressure deduced from eq 1 is

$$p_t = \frac{\sigma}{r} - \frac{1}{2} \frac{K}{r^3} \approx 0 \quad (4)$$

The radius of the tube at coexistence, called the critical radius r_c , is then

$$r_c = \sqrt{\frac{K}{2\sigma}} \quad (5)$$

The critical force f_c is deduced from eq 3, with $r = r_c$

$$f_c = 4\pi\sigma r_c = 2\pi\sqrt{2K\sigma} \quad (6)$$

At this point, it is well to make a few remarks before continuing further:

(1) The capillary force f on the tube is not $2\pi\sigma r$, but $\pi\sigma r$ because one must differentiate the energy (eq 1) at constant volume

$$f = \frac{\partial}{\partial L} (2\pi\sigma r L)_{\Omega} = 2\pi\sigma r + 2\pi L \frac{\partial}{\partial L} (\sigma r)_{\Omega} = \pi\sigma r$$

(2) The shape of the vesicle coexisting with the filament is nearly the shape of a liquid droplet deposited on a fiber of radius $2r_c$, as pointed out by several groups.^{14,16,20} In the region where surface tension dominates, the shape of the vesicles (given by the profile $z(x)$) can be derived from the conservation of the force $f = 2\pi\sigma z \cos \theta$, where θ is related to the slope ($\tan \theta = dz/dx$). The resulting profile $z = z_0 \cosh(x/z_0)$ corresponds to the profile of a meniscus of a liquid rising on a fiber of radius z_0 . For $f = f_c$, the comparison of eq 6 and the one on the conservation of the force shows that $z_0 = 2r_c$. A crossover region of extension r_c relates the vesicle to the tube. In this region, both the surface energy and the membrane bending play a role.

(3) There is a strong analogy between the stretching of vesicles and the stretching of a polymer chain in a bad solvent. The polymer globule is characterized by a surface tension. When it is stretched by a force f , Zhulina and Halperin²¹ have predicted a first-order coil–stretch transition: the globule coexists with an elongated polymer chain.

2. Dynamics: Pulling Force (Evans and Yeung).

The first paper on the dynamics of tether extrusion is due to Evans and Yeung² in the limit where the tube’s radius r is uniform ($r = r_c$). They emphasize the role of the slippage at the birth of the tube and of the dissymmetry induced during extrusion, with the outer layer losing more phospholipids than the inner layer when a tube is extracted. But for the long tubes studied here (in the range of $\sim 100 \mu\text{m}$ to millimeters), the dominant friction is against the solvent and the tension along the tube is no longer uniform. Let us recall the main outcomes of the Evans and Yeung studies. A slightly dehydrated vesicle is first pressurized into spherical form by micropipet suction, as shown in Figure 2. The “manchon” inside the pipet provides a reservoir of lipids. The vesicle is therefore maintained at a constant tension σ_0 . Second, a small adhesive bead is linked to the membrane and is moved at velocity U . The bead is bound to a force transducer, and the pulling force f is measured as a function of the velocity U of extraction.

They study the slow extrusion of short tubes assuming that they are uniform, with a radius r_c given by eq 5. In this limit, the pulling force f can be written as²

$$f = f_c + \eta_s \ln\left(\frac{R_0}{r}\right) U + \frac{K}{2R_0^2} L \quad (7)$$

where f_c is the static pulling force, the second term named “extrusion force” describes the drag between the two monolayers (surface viscosity η_s) pulled at different velocities, and the third term is the restoring force opposing the dissymmetry between the two lipid layers of the vesicle induced by the formation of the tube of length L . These forces are carefully derived in ref 2. A simple scaling interpretation is given in Appendix A.

In the rest of this paper, we will only focus on very long tethers ($L \approx$ hundred microns to millimeters) extruded at high speed. In this case, the friction force along the tube

(20) Bruinsma, R. *Physica A* **1996**, *234*, 249–270.

(21) Halperin, A.; Zhulina, E. *Europhys. Lett.* **1991**, *15*, 417–421.

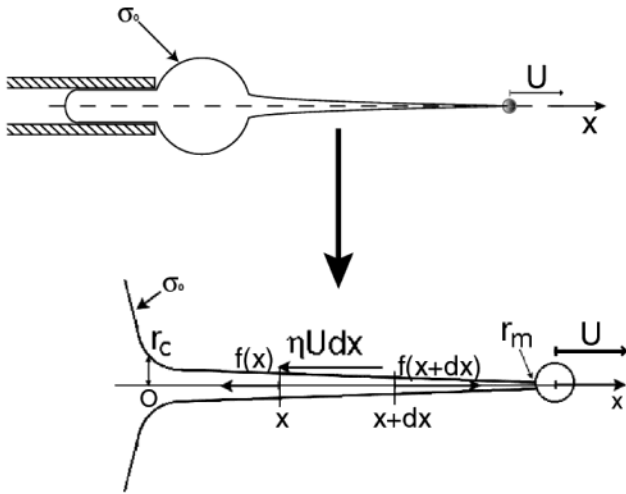


Figure 2. Extrusion of a tube (length L) from a vesicle. The vesicle is maintained at constant stress σ_0 by micropipet suction. An adhesive bead (black dot) is linked to the membrane and is moved at velocity U . Zoom of the profile $r(x)$ of the tube during extraction at constant velocity U by a bead. The friction on the tube generates a gradient of surface tension $\sigma(x)$ from r_m , the tip radius, to r_c , the radius of the tube at the boundary between the vesicle and the tube.

($\sim \eta L \dot{L}$) overcomes the Evans extrusion forces. It implies $L > \eta_s/\eta$ (of order $1 \mu\text{m}$ for water). This friction creates a gradient of surface tension along the tube, and the tube radius is no longer uniform.

III. Dynamics of Pull out by Point Forces

1. Structure of the Stretching Tube (Figure 2). The tube is pulled at constant velocity U by a bead. The length of the tube is $L = Ut$ at time t of extrusion. The friction on the tube generates a gradient of surface tension $\sigma(x)$.

We derive $\sigma(x)$ and the profile of the tube $r(x)$ from the three following equations:

(i) We assume a quasistatic equilibrium. The pressure inside the tube is uniform and equal to zero. Equation 4 leads to

$$2\sigma r = \frac{K}{r} \quad (8)$$

(ii) The flow of lipids is conserved

$$U(x) r(x) = U r_m \quad (9)$$

where r_m is the tip radius and U the (fixed) stretching velocity.

(iii) The balance of mechanical and friction forces can be written as

$$f(x + dx) = f(x) + \zeta_p U(x) dx \quad (10)$$

where ζ_p is the friction coefficient per unit length for a cylinder (length L , radius r) in a flow parallel to the symmetry axis: $\zeta_p = 4\pi\eta/(\ln(L/r) - 1/2)$.

With $f/2\pi = 3/4(K/r) + 1/2\sigma r = K/r$, eqs 9 and 10 lead to

$$-2\pi \frac{K}{r^2} \frac{dr}{dx} = \zeta_p U(x) = \zeta_p U \frac{r_m}{r} \quad (11)$$

The structure of the stretching tube is specified by those three equations, and the two boundary conditions $U(L) = U$ at the extremity and $\sigma(0) = \sigma_0$, that is, $r(0) = r_c$, at the birth of the tube in connection with the “mother” vesicle.

The integral of eq 11, with the boundary condition $r(0) = r_c = (K/2\sigma)^{1/2}$ gives

$$\ln\left(\frac{r}{r_c}\right) = -\frac{\tilde{2}\eta U}{K} r_m x \quad (12)$$

where $\tilde{2}$ is a numerical coefficient including the hydrodynamic interactions: $\tilde{2} \approx 2/\ln(L/r_c)$ if the size of the container (or experiment chamber), denoted d , is larger than the length of the tube. In confined geometries, the hydrodynamic interactions are screened and L is replaced by d .

Equation 12 involves a characteristic length defined by $l^2 = K/\tilde{2}\eta U$. The radius of the tube r_m at the tip is given then by

$$\ln\left(\frac{r_c}{r_m}\right) = \frac{r_m}{r_c} \frac{L}{L_c} \quad (13)$$

where $L_c = l^2/r_c$ is the typical length of variation of the radius (or forces).

With $f = 20 \text{ pN}$ and $U = 100 \mu\text{m s}^{-1}$, we find $L_c \approx 200 \mu\text{m}$. When $L \ll L_c$, eq 13 gives $r_m = r_c$, meaning that the size of the tube is constant. When $L \gg L_c$, eq 13 leads to

$$\frac{r_m}{r_c} \approx \frac{L_c}{L} \ln\left(\frac{L}{L_c}\right) \quad (14)$$

Including all logarithmic corrections in the prefactor, eq 14 leads to $r_m \approx K/\eta UL$.

In the limit $L \gg L_c$, the profile and the membrane tension are given by

$$r = r_c e^{-xr_m/l^2} \quad \sigma(x) = \sigma_0 e^{2xr_m/l^2} \quad (15)$$

The radius of the tube decreases from r_c to r_m , while $\sigma(x)$ increases from σ_0 (the vesicle tension) to $\sigma_m = K/2r_m^2$ at the tip.

The force at this tip f_t , directly deduced from eq 14

$$\frac{f_t}{f_c} \approx \frac{L}{L_c} \approx \frac{\eta U r_c L}{K} \quad (16)$$

increases linearly with (ηUL) , neglecting logarithmic corrections.

Along the tube, the increase of $f(x)$ is deduced from eq 15

$$f(x) = 2\pi \frac{K}{r} = f_c e^{+(x/L_c)(r_m/r_c)} \quad (17)$$

Remark: If the force f_t is maintained constant, eq 16 shows that $L(t)$ increases with $t^{1/2}$ ($\tilde{2}\eta L \dot{L} \approx f_t$, that is, $L \approx [(f_t/\eta)t]^{1/2}$).

2. Tube Retraction. At $t = 0$, we stop the motion of the bead (radius R_b). The tube has a length L_0 . To calculate the retraction $L(t)$, we assume (and we checked in the Appendix) that the tube can relax only from its free end. This is called the “Albatros theorem” by polymer physicists’ “Ses ailes de géant l’empêchent de marcher”, Baudelaire poem.²² A relaxation in the middle would imply a motion of the whole tube and would be extremely slow. On the other hand, the free end (here the bead) can collect the tube very quickly.^{23,24} This explains why we state here

(22) Baudelaire, C. L’Albatros. In *Les Fleurs du Mal*; Spleen et idéal: Paris, 1857.

(23) de Gennes, P. G. *J. Chim. Phys. France* **1967**, *87*, 962.

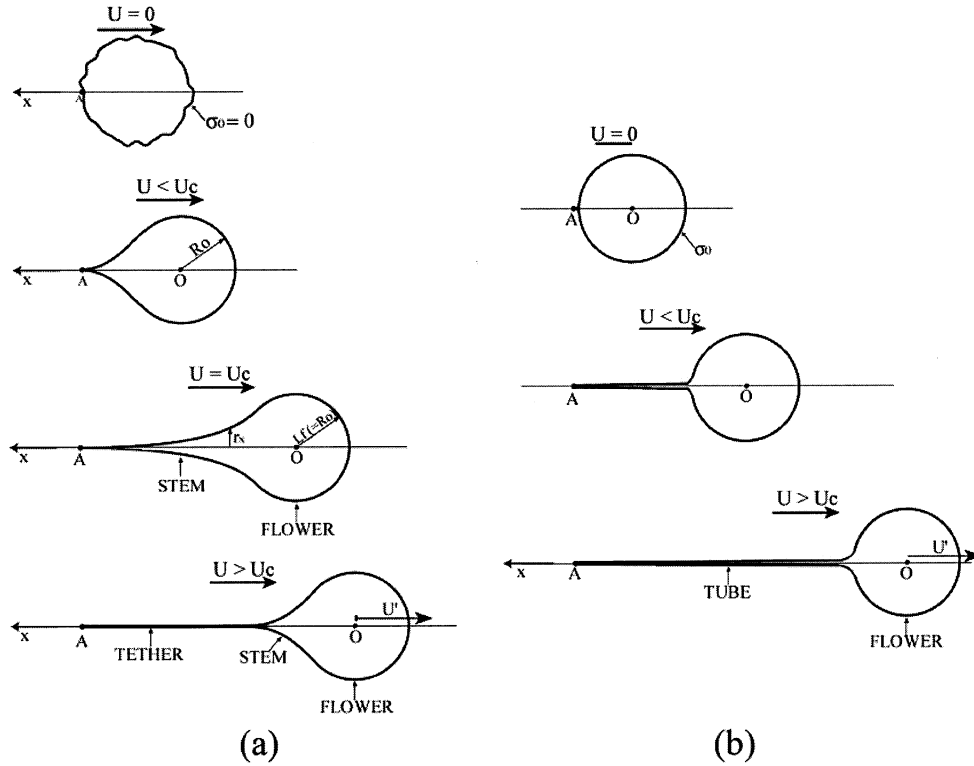


Figure 3. Shapes of vesicles (initial radius R_0) attached by one point A on a solid substrate and submitted to a uniform flow U in two cases: (a) unwinding of floppy vesicles ($\sigma_0 = 0$); (b) unwinding of tense vesicles ($\sigma_i = \sigma_0$).

that the tube is frozen in its initial conformation. We check in the Appendix that the relaxation of the stress σ_x is indeed very slow. We also neglect the viscous losses at the tip: for example, for ultraviscous polymer extrusion, the extraction force is large, but the accumulation of the filament on the bead costs no energy. This can be seen with a filament of honey falling on a piece of bread.²⁵

The relaxation of the tube is then calculated by equating the Stokes friction on the bead, moving at velocity \dot{L} , to the force $f(x = L(t))/2\pi = K/r$ given by eq 17.

$$f(L(t)) = -6\pi\eta R_b \frac{dL}{dt} \quad (18)$$

Notice that following the velocity of retraction leads to a direct measure of $f(x)$ and therefore of $r(x)$. This eq 18 leads to two regimes of retraction:

(i) *Retraction at Constant Velocity.* If $L_0 \ll L_c$ and the force $f \approx f_c$, the tube retracts at constant velocity V_c . This is the case for tense vesicles (σ_0 large) extruded at low velocities U

$$V_c = \frac{f_c}{6\pi\eta R_b} \approx \sigma_0^{1/2} \quad (19)$$

The velocity increases with the vesicle tension σ_0 as $\sigma_0^{1/2}$. The time of retraction is $\tau_{\text{ret}} = L_0/V_c \approx R_b\eta r_c L_0/K$ and decreases as $\sigma_0^{-1/2}$. At the end, when the tube becomes very short, the vesicle shape is a catenoid of size l ($l \approx r_c \ln(R_0/r_c)$), which relaxes very fast with a characteristic capillary time τ_{cap} ($\sigma_0/\eta\tau_{\text{cap}} \approx R_0$).

(ii) *Retraction at Decreasing Velocity.* On the other hand, when $L \gg L_c$, the retraction velocity should decrease with

time from $V_{\text{max}} = f_c/6\pi\eta R_b$ to V_c . Equation 18 with $f(L(t)) = f_c e^{(L/L_c)(r_m/r_c)}$ leads to

$$e^{-Lr_m/l^2} \equiv \frac{2}{3} \frac{U}{R_b} \frac{r_m}{r_c} t + \frac{r_m}{r_c} \quad (20)$$

The retraction time ($L(\tau_{\text{ret}}) = 0$) is given by

$$\tau_{\text{ret}} = \frac{3}{2} \frac{R_b}{U} \frac{r_c}{r_m} \left(1 - \frac{r_m}{r_c}\right) \approx \frac{3R_b\eta L_0 r_c}{K \ln(L_0/L_c)} \quad (21)$$

Equation 21 shows that the retraction time depends weakly (logarithmically) upon the velocity of extrusion U .

IV. Vesicles under Flows

We study first the case of a vesicle attached by one point on a solid substrate and submitted to a uniform flow U . This situation can be realized experimentally by electroosmosis in a charged glass capillary. An electric field creates a plug flow, with a velocity $V \approx \epsilon(E\xi/\eta)$, where ϵ is the dielectric constant and ξ the surface potential. For water, with $E \approx 100 \text{ V}\cdot\text{cm}^{-1}$ and $\xi \approx 100 \text{ mV}$, we get $U \approx 0.5 \text{ mm}\cdot\text{s}^{-1}$.

We consider two cases: (1) unswollen vesicles, with zero surface tension, and (2) swollen vesicles, with an initial tension σ_0 .

1. Pull out from Floppy Vesicles ($\sigma_0 \approx 0$) (Figure 3a). Our aim here is to estimate the critical flow U_c to extrude a tube. We give a scaling description of the shape of the vesicle, ignoring the exact numerical coefficient. We find two regimes:

(i) *Stationary Regime.* Just below the critical current, the vesicle is stationary and composed of two parts, named here the flower and the stem.

The flower is the quasispherical part (size l) dominated by surface tension induced by the flow. The balance of

(24) Buguin, A.; Brochard-Wyart, F. *Macromolecules* **1996**, *29*, 4937–4943.

(25) Skorobogatiy, M.; Mahadevan, L. *Europhys. Lett.* **2000**, *52*, 532–538.

force on the equator ($\sigma = \sigma_f$) is given by

$$\sigma_f l_f = \eta U l_f \quad (22)$$

that is, $\sigma_f \approx \eta U$

The stem is the thinner part controlled by surface tension $\sigma(x)$ and curvature $r(x)$, where x is the coordinate measured from the flower center.

The conditions of zero pressure and force balance give

$$\sigma_x r_x \approx \eta U x \approx \frac{K}{r_x} \quad (23)$$

which leads to

$$r_x = \frac{K}{\eta U x} = \frac{l^2}{x} \quad (24)$$

$$\sigma_x = K \frac{x^2}{l^4}$$

Equation 24 defines a characteristic length l for the variations of r_x . Setting $l_c = R_0$ leads to a critical velocity

$$U_{c0} = \frac{K}{\eta R_0^2} \quad (25)$$

with $K = 4 \times 10^{-20}$, $\eta = 10^{-3}$, and $R_0 = 10 \mu\text{m}$, it gives $U_{c0} = 0.4 \mu\text{m}\cdot\text{s}^{-1}$

U_{c0} is the threshold current to form a tether. The critical force f_c corresponding to $\sigma_f = \eta U_{c0}$ is $f_c = (K\eta U_{c0})^{1/2} = \eta U_{c0} R_0$, which leads also to eq 25.

(ii) *Pulling out* ($U > U_{c0}$). Above U_{c0} , a tube is formed and grows at a velocity $U' = dL/dt$. The driving force on the flower is

$$f = \eta(U - U')R_0 \quad (26)$$

and the stress $\sigma = \eta(U - U')$. The condition $f = f_c$ leads to

$$U - U' = U_{c0} \quad (27)$$

2. Pull out from Tense Vesicles ($\sigma_0 > \eta U_{c0}$) (**Figure 3b**). The situation described above was limited to floppy depressurized vesicles, with a residual tension less than $\eta U_{c0} \approx K/R_0^2 \approx 10^{-7} \text{mN}\cdot\text{m}^{-1}$. We study here the extrusion of tubes from a slightly tense membrane with $\sigma_0 \gg \eta U_{c0}$ (**Figure 3b**).

(i) *Threshold Current U_c : Stationary Regime*. The Stokes force on the vesicle (radius R_0) must be equal to the critical force f_c corresponding to σ_0 . This defines the critical current U_c

$$\eta U_c R_0 \approx \sqrt{K\sigma_0} \quad (28)$$

U_c defined by eq 28 can also be written as

$$U_c = \sqrt{U_{c0} V^*} \quad (29)$$

where $V^* = \sigma_0/\eta$ is a capillary velocity.

The shape of the flower is quasispherical, with a small meniscus of typical size $r_c = (K/2\sigma_0)^{1/2}$.

At U_c , in the stationary regime, the profile of the stem is given by eq 11 with $U_x = U$ all along the tube at rest.

It leads to

$$\frac{1}{r_x} - \frac{1}{r_c} = \frac{x}{l^2} \quad (30)$$

with $l^2 = K/2\eta U_c \approx r_c R_0$.

(ii) *Extrusion*: $U > U_c$. Above U_c , the vesicle is extruded at a velocity $U' = \dot{L}$. The driving force of unwinding is

$$\eta(U - U')R_0 = f_c \quad (31)$$

showing that

$$U - U' \equiv U_c \quad (32)$$

(iii) *Profile of the Extruded Tube*. As the tube gets very long, one shall also include the friction on the tube. In the reference frame of the globule, the velocity of the tube is called u'_x . At the tip, $u'_L = U'$ and $r = r_m$. The lipid conservation equation becomes $r_m U' = r_x u'_x = r_c u'_0$, where u'_0 is the velocity of extrusion at the neck between the vesicle and the tube. The balance of forces on a tube element dx (**Figure 2**) including the friction of the solvent moving at a relative velocity $U - (U' - u'_x)$ against the tube becomes $\zeta_p(U - U'(1 - r_m/r)) dx + f(x) = f(x + dx)$.

With $f(x)/2\pi = K/r$, we get $-Kr'/r^2 = 2\eta(U_c + (U - U_c) - r_m/r)$.

For $U \approx U_c$, the profile is given by eq 30. For $U \gg U_c$, we find $\ln r/r_c = -2\eta U r_m x/K$.

Setting $r = r_m$ for $x = L$ leads to $r_m/r_c = e^{-Lr_m/l^2}$, that is, $r_m/r_c \approx L\sigma/L \ln U/U_c$, setting, as before, $l^2 = K/2\eta U$ and $L_c = l^2/r_c$.

3. Role of Increasing Surface Tension. The extrusion of the tube, especially at low σ values corresponding to “thick” tubes, decreases the excess surface, and the tension of the vesicle starts to increase. According to eq 29, U_c also increases and $\dot{L} = U'$ decreases down to $U' = 0$. The vesicle is then in a stationary regime and the length of the tube remains constant. The maximal stress reached is given by eq 28 with $U_c = U$ and $\sigma_\infty = \eta^2 U^2 R_0^2/K$ ($\approx 2 \times 10^{-5} \text{N}\cdot\text{m}^{-1}$ for $U = 100 \mu\text{m}\cdot\text{s}^{-1}$ and $R_0 = 10 \mu\text{m}$).

4. “Stop Flow”: Vesicle Relaxation (Figure 8). Here the attachment point A is fixed, and the vesicles relax by “eating” their own tube. We assume as before that the tube is “petrified” in its building configuration. The gradient of surface tension can relax only by a slow diffusive mode, as shown in the Appendix. The fastest process is the relaxation by the free end, here the flower.

As the vesicle eats the tube, its radius R_0 does not change. The vesicle moves at the velocity \dot{L} of the tube retraction. The friction forces on the vesicle balance the mechanical force $f(x=L(t))$:

$$-6\pi\eta R_0 \dot{L} = f(x=L_0 - L(t)) \quad (33)$$

At this point, we must specify the history of the tube extraction:

If the vesicle under flow has reached a stationary state ($U = U_c$), the force is given by

$$f(x=L_0 - L(t)) = 2\pi\tilde{2}\eta U_c(L_0 - L(t)) + 6\pi\eta R_0 U_c = -6\pi\eta R_0 \dot{L}$$

The solution for $L(t)$ is

$$\ln \frac{\tilde{L}_0 - L(t)}{\tilde{L}_0 - L_0} = \frac{\tilde{2}}{3} \frac{U_c t}{R_0} \quad (34)$$

where $\tilde{L}_0 = 3/2 R_0 + L_0$.

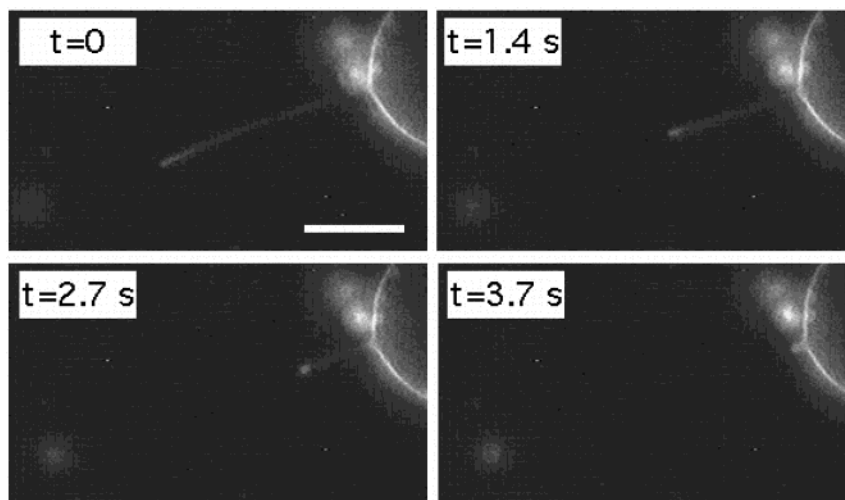


Figure 4. Fluorescence videomicrographs of a tube retraction sequence after extraction by mechanical force. The vesicle is maintained by the pipet, and the bead (invisible) is moving back to the vesicle. The bar length is $50 \mu\text{m}$.

The retraction time $\tau_{\text{ret}} \approx \frac{3}{2}(R_0/U_c) \ln(L_0/R_0)$ is independent of the viscosity of the liquid. This can be checked by using a water/glycerol mixture: the threshold velocity decreases as η^{-1} , while τ_{ret} should remain constant.

V. Observations of Tube Retractions

Here, we present our experimental results and compare them with previously described theoretical predictions. Tether formation was achieved by two different methods: (1) mechanical pulling and (2) electroosmotic flow. Retraction dynamics studies were performed in both cases. Mechanically extruded tubes were obtained by micropipet manipulation. This technique allows a fine control of membrane tension and provided us with a detailed description of the retraction velocity as a function of membrane tension. Electroosmotically extruded tubes were obtained from flaccid (unsucked) vesicles. By forming tubes under flows, we were able to monitor the exponential retraction dynamics predicted in the theoretical section.

1. Micromanipulation Experiments: Retraction of Tubes Pulled out at Constant Velocities U . Figure 4 displays snapshots of a tether retraction sequence which starts when the suction pressure is released in the pipet. A $5 \mu\text{m}$ glass microbead is glued to the free end of the tube. For the time course of complete retraction (from <1 to 5 s), the gravity of the bead (≈ 50 fN) is negligible and the motion of the bead which is pulled by the shrinking tube was observed to be straight. The time dependence of the tube length was obtained by simultaneously tracking the interdistance between the two ends of the tube and by a direct measurement of the tube length after applying appropriate thresholds to the images. Despite a weak signal, a spatial resolution better than $1 \mu\text{m}$ was thus achieved, while the temporal resolution was fixed by the video rate (25 Hz).

From the theoretical description presented above, three parameters are supposed to play a key role in the dynamics of tube retraction: the membrane tension, σ , the solvent viscosity, η , and the extraction velocity, U . This reveals that the history of tube formation influences the dynamics of retraction. In all our experiments, we selected PBS buffer (phosphate buffered saline) as a solvent ($\eta = 10^{-3}$ Pa·s) to fill in the manipulation chamber.

In a first set of measurements, tethers were extracted at a constant and low speed, $U = 15 \mu\text{m/s}$, which sets the characteristic length scale, L_c , between a few hundredths of a micron and several millimeters for vesicle tensions

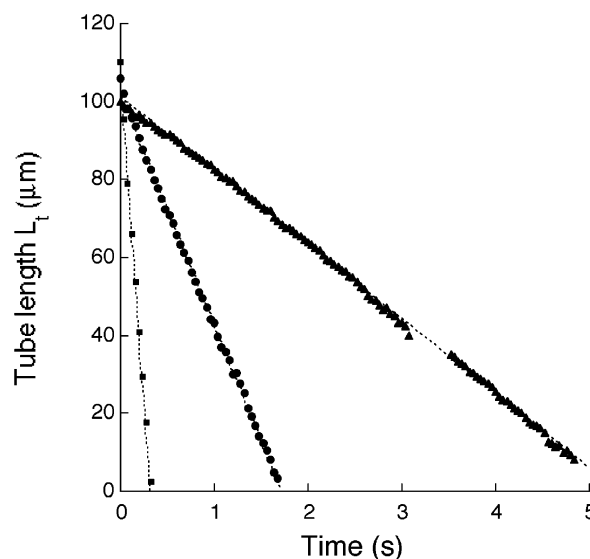


Figure 5. Representative temporal evolution of tube length during retraction for different vesicle tensions: (▲) $\sigma = 10^{-2}$ $\text{mN}\cdot\text{m}^{-1}$; (●) $\sigma = 10^{-1}$ $\text{mN}\cdot\text{m}^{-1}$; (■) $\sigma = 0.3$ $\text{mN}\cdot\text{m}^{-1}$.

in the 10^{-3} to 0.5 mN/m range. Data were obtained from more than 20 vesicles (or tethers) with radii R_v ranging from 10 to $30 \mu\text{m}$ and tether lengths L_t between 50 and $100 \mu\text{m}$. The radius of the beads, R_b , was kept constant and equal to $2.45 \mu\text{m}$. Figure 5 shows the time evolution of tube lengths for three different membrane tensions fixed by pipet aspiration. Initial lengths were on the order of $100 \mu\text{m}$. Over the whole sequence, tube retraction occurred at constant velocity, V_c . More interesting, V_c was found to increase with σ . From flaccid ($\sigma \approx 10^{-3}$ mN/m) to tense vesicles ($\sigma = 0.5$ mN/m), retraction speeds span over 1 order of magnitude. In Figure 6, we plot the square of V_c versus the membrane tension. For each data point, two to five vesicles were evaluated. At low tensions, the uncertainty is mainly in the estimate of σ . At higher tensions, retraction occurred within less than 1 s, which yields higher uncertainty on velocity measurements. The graph was fitted with a linear function, and the slope was found to be equal to 3.56×10^{-4} $\text{N}^{-1}\cdot\text{m}^3\cdot\text{s}^{-2}$. This dependence is in good agreement with eq 19, which predicts a linear variation of V_c^2 with σ for initial tube lengths below L_c , with a prefactor equal to $2\kappa/(9\eta^2 R_b^2) = 1.48 \times 10^{-4}$ $\text{N}^{-1}\cdot\text{m}^3\cdot\text{s}^{-2}$.

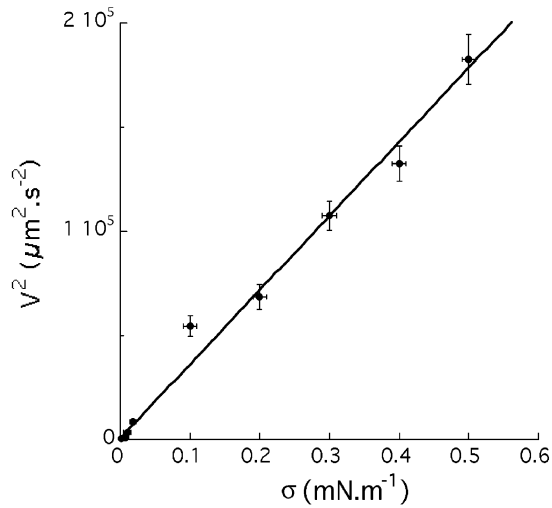


Figure 6. Square of the retraction velocity versus membrane tension in the regime of constant retraction velocity. Linear fit yields $V^2 = (3.56 \times 10^{-4})\sigma$.

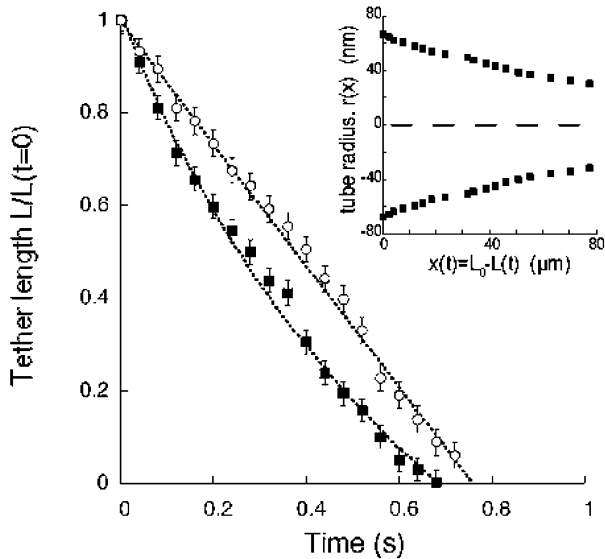


Figure 7. Influence of the extraction speed on the retraction dynamics when tubes are pulled out by mechanical forces: Tube length versus time. For (○) $U = 15 \mu\text{m/s}$, the retraction velocity is constant. For (■) $U = 400 \mu\text{m/s}$, the best fit was obtained for $L = -0.89 \log_e(t + 0.32)$. Inset: Shape $r(x)$ of the tube extracted at $U = 400 \mu\text{m/s}$, derived from the retraction curve according to eq 18.

In a second set of experiments, we attempted to form tethers at higher speeds. The main difficulty came from the fact that fast and irregular extrusion led to a pearling instability which has already been observed and studied by others.²⁶ Extraction speeds of $400 \mu\text{m/s}$ could be reached on about 10 weakly aspirated vesicles. Figure 7 displays the retraction dynamics of two “identical” tethers pulled respectively at low speed ($U = 15 \mu\text{m/s}$) and high speed ($U = 400 \mu\text{m/s}$). By “identical”, we mean that the tethers were formed from equally tense vesicles ($\sigma = 10^{-2} \text{mN/m}$) and that their initial lengths were comparable ($\approx 70 \mu\text{m}$). Lengths were normalized to $L(t=0)$ for the sake of comparison. While the time dependence of the slowly extruded tube could be fitted with a linear function, as shown in the previous paragraph, there was a significant deviation from linear behavior for the tethers which were

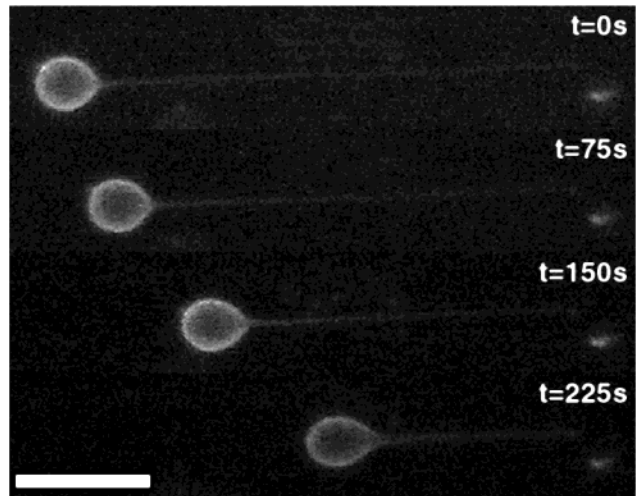


Figure 8. Fluorescence videomicrographs of a tube retraction sequence after extraction by electroosmotic flow. The tube is attached to a point (microbead) on the substrate, and the vesicle is moving back by eating its own tube. The bar length is $20 \mu\text{m}$.

extracted at high speed. A better fit was obtained using the logarithmic function derived from eq 20: $L = -\alpha \log_e(\beta t + \gamma)$. The choice of this fitting function was validated by the fact that $L_0 \gg L_c \approx 20 \mu\text{m}$ for $U = 400 \mu\text{m/s}$. Values for the fitting parameters were $\alpha = 0.89$, $\beta = 1$, and $\gamma = 0.32$. These values are consistent with theoretical predictions, since the combination of eq 20 with the definition of L_c shows that L_0/L_c is equal to the product $\alpha\gamma = 0.28$ (which is indeed found for $L_0 = 70 \mu\text{m}$ in Figure 7). From this $L(t)$ retraction curve, we have derived the shape $r(x)$ of the tube according to eq 18. As predicted theoretically, the radius is found to be not constant and decreasing from the vesicle to the tip.

2. Electroosmosis Experiments: Retraction of Tubes Pulled out under Flow. Figure 8 displays fluorescence video-micrographs of a tether retraction sequence which starts when the voltage was set to zero. First, the tube was extracted under a current $U = 0.11 \mu\text{m/s}$, and we waited till the stationary regime was reached. Contrary to mechanical experiments, the end of the tube is here attached to the substrate, while the vesicle is pulled back by the shrinking tube. Another major difference with the micropipet experiments is that these electroosmosis experiments were performed in a mixture of PBS and glycerol ($v/v = 34/66$). The higher viscosity of the medium ($\eta = 32 \text{cP}$) was useful to avoid any significant effect of the neighboring surface on the hydrodynamics around the tube. As a consequence, tube retractions typically occurred within several minutes for initial tube lengths L_0 larger than $50 \mu\text{m}$ (Figure 8). More interesting, the time dependence of the tether length was found to be significantly different from the one observed in the micropipet experiments. In Figure 9, we plot $L(t)$, the time evolution of tube length. The retraction velocity is observed to be not constant. More precisely, we fit the experimental data using eq 34. An excellent agreement is observed, and the fitting parameters are $\bar{L}_0 = 89.8 \mu\text{m}$ and $U_c = 0.099 \mu\text{m}\cdot\text{s}^{-1}$. These values are consistent with the analytical expression of \bar{L}_0 given by eq 34 and the experimental value of U_c at the stationary regime ($R_0 = 14.8 \mu\text{m}$ with $K = 4 \times 10^{-20} \text{J}$ and $U_c = U = 0.11 \mu\text{m}\cdot\text{s}^{-1}$).

The nontrivial influence of the surface proximity coupled with the viscosity of the surrounding medium and the dependence of U_c upon the electric field and surface tension are being currently investigated and will be described in detail in a forthcoming paper.

(26) Bar-Ziv, R.; Moses, E.; Nelson, P. *Biophys. J.* **1998**, *75*, 294–320.

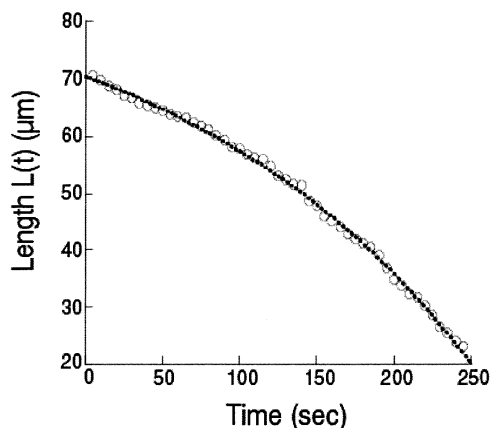


Figure 9. Length of retracting tube versus time when tubes are pulled out under electroosmotic flows. The dotted line is the fitting curve derived from eq 34.

VI. Concluding Remarks

We have described the dynamics of extrusion and retraction of lipid nanotubes formed either by local forces or by flows.

1. Extrusion by Local Forces. A small bead (radius R_b) is linked to the membrane of the vesicle (tension σ imposed by a pipet suction) and pulled out at velocity U . In this way, we have shown that, to achieve well calibrated tubes of length L , the extrusion velocity must be less than $U_c \approx f_c/\eta U$, which compares a characteristic friction on the tube to the static threshold extrusion force f_c . At higher speeds, the tube is no longer uniform: going from the vesicle end to the tip (bead end), the stretching force $f(x)$ increases from f_c to f_t , while the tube radius decreases and the membrane stress increases. The force $f(x)$ is directly measured by looking at the relaxation of the tube, terminated by the bead. The retraction by the free end is much faster than the relaxation of the gradient $f(x)$ along the tube. The force field $f(x)$ is “frozen”. The motion of the bead results simply from a balance between the Stokes friction on the bead moving at the retraction velocity \dot{L} and the “frozen” force $f(x)$. Our experiments on tube relaxations are in agreement with these predictions: for tubes extruded at low velocities, the retraction velocity is constant and scales as $\sigma^{1/2}$. In the opposite limit of fast extrusion, the retraction velocity slows down and the law for $L(t)$ fits our theoretical predictions.

2. Extrusion by Flows. Vesicles, linked locally by a bead to a substrate, are unwound by flows (velocity U). Above a threshold velocity U_c , a tube is formed and its length increases up to a stationary regime: here, unlike the case for extrusion by local forces, the tension of the vesicle is not maintained constant; rather, it increases to reach a value σ_∞ such that $U = U_c(\sigma_\infty)$. Experiments to measure the relation between σ_∞ and U are underway ($\sigma_\infty \propto U^2$ is predicted).

Tubes of lengths varying from several microns to millimeters at high flows can be built. This type of tube extrusion is extremely easy to set up and does not require any micromanipulations, as opposed to all the techniques used previously. A dispersion of sticking beads is deposited on a substrate. Vesicles attach spontaneously to the beads, and a flow is applied either by a pressure gradient or by an electrical field.

We see two applications of this work:

(1) This unwinding of giant vesicles induced by flows can be used to stretch living cells as well, and experiments on red blood cells are underway. This will allow us to test the mechanical response of the cytoskeleton (spectrin

network) induced by the stretching of the membrane, in a well-controlled geometry.

(2) The extrusion of a tube may be a way to encapsulate proteins or DNA inside tubes of section varying from hundreds of nanometers to several microns. DNA adsorbs slightly on the membrane of our giant vesicles despite the same sign of electrical charges (negative). This condition of weak binding may be favorable to extrude DNA membrane complexes and achieve one-dimensional DNA structures, encaged in a tube of well-controlled geometry. This may have numerous applications, in particular to follow chemical binding reactions of proteins with DNA.

VII. Experimental Section

1. Vesicles. Phospholipid vesicles of various compositions were used for the sake of practical convenience. In experiments dealing with tubes pulled out at constant velocity, vesicles were made from a mixture of EPC (egg phosphatidylcholine, Avanti Polar Lipids Inc.), a biotinylated lipid, namely DOPE N cap Biotinyl (Avanti Polar Lipids Inc.), and a fluorescent lipid, Bodipy 530-C5-HPC ($\lambda_{\text{excitation}} = 530$ nm, $\lambda_{\text{emission}} = 550$ nm, Molecular Probes) in a 98/1/1 weight ratio. The biotinylated lipid was used to make vesicles sticky for streptavidin-coated beads. The fluorescent lipid allowed visualization of submicronic membrane tubes by fluorescence microscopy. In experiments carried out on tubes extracted under flows, vesicles were made from dioleoylphosphatidylcholine (DOPC). In this case, fluorescent labeling was performed by perfusion of Di6-ASPPS (1% v/v in ethanol, $\lambda_{\text{excitation}} = 465$ nm, $\lambda_{\text{emission}} = 560$ nm, kindly provided by Mireille Blanchard-Desce, Université de Rennes, France). This fluorophore appeared to be less sensitive to photobleaching and thus more convenient for long periods of observation.

In both types of experiments, vesicles were prepared using the electroformation method described in ref 27. Electroswelling was carried out in a solution of sucrose to enhance contrast in DIC (differential interference contrast) microscopy observations. Osmolarity was set at 148 mOsm so that vesicles were initially flaccid. The vesicles obtained in this way were usually large, with diameters from 10 to 100 μm , and the majority of them appeared to be unilamellar. In the electroosmosis experiments, glycerol was added to the external solution in order to increase the viscosity of the medium (see section V.2)

2. Microbeads. For retraction experiments performed on tethers extruded by mechanical force, we used homemade streptavidin-coated glass beads as handles. Borosilicate microspheres (4.9 ± 0.5 μm in diameter, Duke Scientific Corp) were chemically modified following a three-step procedure described elsewhere.²⁸ Briefly, after activation with an aminosilane (*N*-[3-(trimethoxysilyl)propyl]ethylenediamine, Sigma-Aldrich) and reaction with a biotinylated cross-linker (NHS-PEG³⁴⁰⁰-biotin, Shearwater Polymers), beads were finally coated with streptavidin (Jackson ImmunoResearch Laboratories Inc.).

For experiments carried out on tethers formed by electroosmosis, we used amino-functionalized beads as attachment points to the substrate for vesicles. These amino-beads were kindly provided by Spherotech (AM-10-10, 1.27 μm in diameter). They were used after washing and resuspension in PBS (phosphate buffered saline) at high dilution.

3. Mechanical Experiments: Micromanipulation. Micropipets were formed by pulling needles from glass capillary tubing using a horizontal laser pipet puller (P-2000, Sutter Instrument Co.) and by breaking off the tips with a microforge at the desired inside diameters (2–10 μm). All the mechanical experiments were performed in a small chamber made of two cover slides separated by 2 mm.²⁹ The chamber was mounted on an inverted microscope (Axiovert 200, Zeiss) equipped with a 100-W Hg lamp, narrow (± 20 nm) band-pass filters, a 100 \times Plan-Apochromat oil immersion objective (N.A. 1.4), and an intensified

(27) Dimitrov, D. S.; Angelova, M. I. *Bioelectrochem. Bioenerg.* **1988**, *19*, 323–336.

(28) Merkel, R.; Nassoy, P.; Leung, A.; Ritchie, K.; Evans, E. *Nature* **1999**, *397*, 50–53.

(29) Needham, D.; Zhelev, D. V. *Surfactant Sci. Ser.* **1996**, *62*, 373–444.

camera (Lhesa). Beads and vesicles were manipulated in the chamber with micropipets mounted on piezodriven micromanipulators (Physik Instrumente).

The suction pressure in the vesicle-holding pipet was controlled by adjusting the height of a water-filled reservoir connected to the back of the pipet. A pressure transducer (Validyne, DP103) was used to measure the applied pressure. Typical pressures were in the range 0–0.1 Pa. Membrane tension σ was computed from the formula²⁹ $\sigma = \Delta P R_p / [2(1 - R_p/R_v)]$, where ΔP is the applied suction pressure, R_p is the inner radius of the pipet, and R_v is the radius of the portion of the vesicle outside of the pipet.

In preparation for membrane tether extrusion, the chamber was filled with a suspension of biotinylated fluorescent vesicles at one side and with a diluted suspension of avidin-coated microbeads at the other side. A single vesicle was selected and aspirated into one pipet, while a bead was picked up by the second pipet. To form a tether, the bead was moved into contact with the vesicle and allowed to stick to it. The bead was then retracted at constant speed up to distances of about 100 μm . When the suction pressure in the bead-holding pipet was released, the bead was pulled back to the vesicle by the retracting tether. Retraction sequences were recorded in real time with a VCR.

4. Electroosmosis Experiments. The electroosmosis chamber was assembled by sandwiching two pieces of a silicone sheet (Gelpack TM, 400 μm thick) between two clean glass cover slides. Typical sizes of the chamber were 20 \times 2 mm². The chamber was mounted on an inverted microscope (Axiovert 135, Zeiss) equipped for fluorescence observation (as described in the previous paragraph). Amino-beads (1.27 μm in diameter) were first seeded at low surface density (about 1 bead/500 μm^2) on the bottom of the chamber. After washing and exchanging PBS with a PBS/glycerol (v/v 34/66) solution, vesicles were incorporated at one end of the channel. The electric field, E , was applied by connecting two platinum wires to a low voltage generator. Typical values of E were in the range from 1 to 20 V $\cdot\text{cm}^{-1}$. In all the experiments, the voltage was increased gradually until the desired length of the tube was reached. Retraction dynamics was monitored by switching off the voltage at time $t = 0$, and the sequences were recorded with a VCR. We took into account possible spatial variations of the glass surface potential by performing a calibration of the current U as a function of E after each extrusion–retraction experiment. Fluorescent microbeads served as flow tracers, and we found out that typical values for U were in the range 0.05–10 $\mu\text{m}\cdot\text{s}^{-1}$.

5. Image Analysis. After digital capture of sequences of interest (Matrox Meteor-II/digital frame grabber), the images were analyzed using homemade software to derive the tube length as a function of time.

Acknowledgment. We thank P. Bassereau, J. Prost, and J. F. Joanny for fruitful discussions. The work was supported by the Institut Curie and the CNRS through the “Nano-Objet Individuel 2001” program. One of us (O.R.) thanks the ARC for the one-year fellowship (n° MI/MLD/CM-P01/5).

Appendix A: Extrusion Force at the Vesicle/Tube Interface (Figure 10)

We present here a simple view of the extrusion force derived carefully in ref 2:

$$f = f_c + \eta_s \ln(R_0/r) + KL/2R_0^2 \quad (\text{A1})$$

The lipid fluxes J_1 and J_2 flowing out of the external and internal lipid layers (thickness h) during the extraction of the tube are

$$J_1 = 2\pi(r + h)h\dot{L} \quad (\text{A2})$$

$$J_2 = 2\pi r h \dot{L} \quad (\text{A3})$$

If n_+ is the number of lipids in the outer membrane and

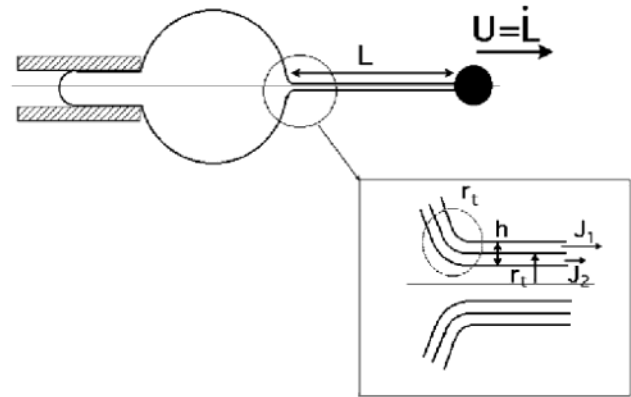


Figure 10. Extrusion of a tube (length L) from a vesicle. The vesicle is maintained at constant stress σ by micropipet suction. An adhesive bead (black dot) is linked to the membrane and is moved at velocity U . The inset represents a zoom of the boundary between the tube and the vesicle where $r_t = r$ is the tube radius, h the thickness of the lipid bilayer, and J_1 and J_2 the lipid fluxes flowing out of the external and internal lipid layers during the extraction of the tube.

n_- is the number in the inner membrane, lipid conservation leads to

$$-\frac{d}{dt}(n_+ - n_-) = \frac{J_1 - J_2}{v} = 2\pi h^2 \frac{\dot{L}}{v} \quad (\text{A4})$$

where v is a lipid molecular volume.

This dissymmetric pumping creates a force with both an elastic and a viscous component:

1. “Elastic” Force. The dissymmetry between the densities of the two monolayers leads to a spontaneous curvature $c_0 = n_+ - n_- / \bar{n}h$ and an energy $E \approx Kc_0^2 R_0^2$. Using eq A4, it leads to $E \approx KL^2/R_0^2$. The associated restoring force $F = \partial E / \partial L$ scales such as KL/R_0^2 .

2. Interlayer Drag Force. The friction between the sliding monolayers moving at velocities v_1 and v_2 can be estimated from the viscous dissipation $T\dot{S} = \dot{L}f_v = \eta_M((v_1 - v_2)^2/h^2)hr^2$, where we have assumed that the drag force is limited to an area of typical size r . $v_1 - v_2$ is related to $J_1 - J_2$ by $J_1 - J_2 = 2\pi r h(v_1 - v_2)$. With $v_1 - v_2 \approx h\dot{L}/r$, we get $f_v = \eta_M \dot{L}h$. The measure of f_v ²⁹ leads to a lipid viscosity $\eta_M \approx 500 \eta_{\text{water}}$.

Appendix B: “Frozen” Forces Approximation

We have assumed that the relaxation of the gradient of surface tension along the tube was slow, compared to the destruction by the free end. To justify this hypothesis, we look at the relaxation of a periodical modulation of the stress $\sigma(x)$ or of the density $\Gamma(x)$

$$\sigma(x) = \sigma_0 + \sigma_1 e^{iqx} e^{-t/\tau_q} \quad (\text{B1})$$

$$\Gamma(x) = \Gamma_0 + \Gamma_1 e^{iqx} e^{-t/\tau_q} \quad (\text{B2})$$

For a plane surface, this mode has been studied by Lucassen³⁰ in the case of a monolayer, floating on a liquid bath of thickness e . A gradient of surface tension $\sigma' = d\sigma/dx$ gives rise to a shear flow $V = V_s x/e$. The viscous stress at the interface must balance the surface stress:

$$\eta \frac{V_s}{e} = \frac{d\sigma}{dx} \quad (\text{B3})$$

(30) Lucassen, J. *Chem. Eng. Sci.* **1972**, *27*, 1283.

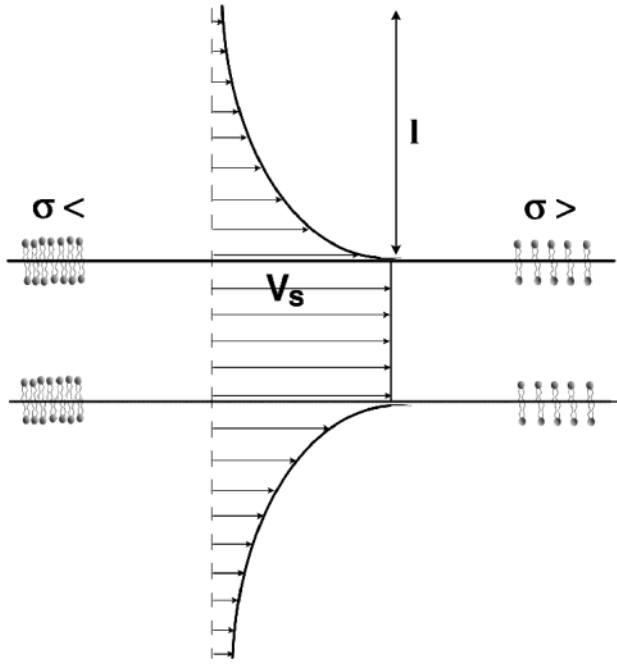


Figure 11. For a curved surface of radius r , the flows inside the tube are plug flows (velocity V_s) and outside they extend over the penetration length l .

The lipid flow is thus

$$J = \Gamma V_s = \Gamma \frac{e}{\eta} \frac{d\sigma}{dx} = \Gamma \frac{e}{\eta} \frac{d\sigma}{d\Gamma} \frac{d\Gamma}{dx} \quad (\text{B4})$$

Equation B4 defines a diffusion coefficient

$$D = E \frac{e}{\eta} \quad (\text{B5})$$

where $E = \Gamma d\sigma/d\Gamma$ is the elastic modulus associated to the compression of the monolayer.

The Lucassen modes are derived from eq B4 and the mass conservation

$$\frac{d\Gamma}{dt} + \text{div } J = 0 \quad (\text{B6})$$

The modes are diffusive ($1/\sigma_q = Dq^2$), with a diffusion coefficient $D = Ee/\eta$. We can also find this result from a transfer of elastic energy $F_q = 1/2 E (du/dx)^2$ (where u is the molecular longitudinal displacement) into viscous losses.

$$\dot{F}_q = Eq^2 u \dot{u} = -\eta \left(\frac{\dot{u}}{e} \right)^2 e \quad (\text{B7})$$

For a curved surface of radius r , the flows inside the tube are plug flows (Figure 11) and outside they extend on the

penetration length ($1/l_p^2 = q^2 + \rho\omega/\eta$). The energy transfer per unit length can be written as

$$\dot{F}/m = rEq^2 u \dot{u} = - \left(\eta_M h r \dot{u}^2 q^2 + \eta \frac{\dot{u}^2}{l_p^2} l_p^2 \right) \quad (\text{B8})$$

where we included dissipation inside the bilayer (viscosity η_M) and in the surrounding liquid.

Equation B8 leads to a dispersion relation

$$Erq^2 = (\eta_M h r q^2 + \eta) \frac{1}{\tau_q} \quad (\text{B9})$$

This equation defines a threshold wave vector $q_c^2 = \eta/\eta_M h r$. At very short wavelengths, the mode relaxes with a characteristic time $\tau = \eta_M h/E$. At the long wavelengths studied here, the mode is diffusive

$$\frac{1}{\tau_q} = Dq^2 \quad (D = E \frac{r}{\eta}) \quad (\text{B10})$$

This mode is similar to the diffusive Lucassen mode, with the radius of the tube instead of the thickness of the shallow liquid bath.

If we look at the relaxation of a gradient extending over the tube length L , the relaxation time T_{rel} is given by

$$T_{\text{rel}} = \frac{\eta L^2}{Er} \quad (\text{B11})$$

We must compare this time to the retraction time. In the case of the retraction of a tube attached to a bead (paragraph IV.1), the velocity of retraction is $V = \sigma r/\eta R_b$. The retraction time is then

$$T_{\text{ret}} = \frac{L}{V} = \eta \frac{R_b}{\sigma r} L \quad (\text{B12})$$

Assuming $E \approx \sigma$, the comparison of eqs B11 and B12 shows that

$$\frac{T_{\text{rel}}}{T_{\text{ret}}} \approx \frac{L}{R_b} \quad (\text{B13})$$

As long as $L \gg R_b$, the tube is destroyed by its free end and the forces along the tube are frozen. To check this result, we have performed the following experiment: we extruded a vesicle (tension σ_1) at a fast velocity U , and we released it suddenly: the velocity of retraction is not uniform. On the other hand, if we keep the bead at rest for a while (few minutes) and let it go, we observe a retraction at uniform velocity, showing that the tension has relaxed to σ_1 all along the tube.

LA026236T